All solid-state spectral broadening: an average and peak power scalable method for compression of ultrashort pulses

Marcus Seidel,[1,*] Gunnar Arisholm,[2] Jonathan Brons,[1] Vladimir Pervak,[3] and Oleg Pronin[1]

[1]*Max-Planck-Institut fr Quantenoptik, Hans-Kopfermann-Str. 1, D-85748 Garching, Germany*
[2]*FFI (Norwegian Defence Research Establishment), P. O. Box 25, NO-2027 Kjeller, Norway*
[3]*Ludwig-Maximilians-Universität München, Am Coulombwall 1, D-85748 Garching, Germany*

[*]*marcus.seidel@mpq.mpg.de*

Abstract: Spectral broadening in bulk material is a simple, robust and low-cost method to extend the bandwidth of a laser source. Consequently, it enables ultrashort pulse compression. Experiments with a 38 MHz repetition rate, 50 W average power Kerr-lens mode-locked thin-disk oscillator were performed. The initially 1.2 μJ, 250 fs pulses are compressed to 43 fs by means of self-phase modulation in a single 15 mm thick quartz crystal and subsequent chirped-mirror compression. The losses due to spatial nonlinear effects are only about 40 %. A second broadening stage reduced the Fourier transform limit to 15 fs. It is shown that the intensity noise of the oscillator is preserved independent of the broadening factor. Simulations manifest the peak power scalability of the concept and show that it is applicable to a wide range of input pulse durations and energies.

OCIS codes: (140.7090) Ultrafast lasers; (190.3270) Kerr effect; (190.7110) Ultrafast nonlinear optics; (320.0320) Ultrafast optics; (320.5520) Pulse compression.

References and links

1. N. Bloembergen, "From nanosecond to femtosecond science," Rev. Mod. Phys. **71**, S283–S287 (1999).
2. A. H. Zewail, "Femtochemistry: atomic-scale dynamics of the chemical bond," J. Phys. Chem. A **104**, 5660–5694 (2000).
3. S. T. Cundiff and J. Ye, "*Colloquium* : Femtosecond optical frequency combs," Rev. Mod. Phys. **75**, 325–342 (2003).
4. R. R. Gattass and E. Mazur, "Femtosecond laser micromachining in transparent materials," Nature Photon. **2**, 219–225 (2008).
5. S. T. Cundiff and A. M. Weiner, "Optical arbitrary waveform generation," Nature Photon. **4**, 760–766 (2010).
6. M. Hentschel, R. Kienberger, C. Spielmann, G. A. Reider, N. Milosevic, T. Brabec, P. Corkum, U. Heinzmann, M. Drescher, and F. Krausz, "Attosecond metrology," Nature **414**, 509–513 (2001).
7. F. Krausz and M. I. Stockman, "Attosecond metrology: from electron capture to future signal processing," Nature Photon. **8**, 205–213 (2014).
8. A. Schiffrin, T. Paasch-Colberg, N. Karpowicz, V. Apalkov, D. Gerster, S. Muhlbrandt, M. Korbman, J. Reichert, M. Schultze, S. Holzner, J. V. Barth, R. Kienberger, R. Ernstorfer, V. S. Yakovlev, M. I. Stockman, and F. Krausz, "Optical-field-induced current in dielectrics," Nature **493**, 70–74 (2013).
9. T. T. Luu, M. Garg, S. Y. Kruchinin, A. Moulet, M. T. Hassan, and E. Goulielmakis, "Extreme ultraviolet high-harmonic spectroscopy of solids," Nature **521**, 498–502 (2015).
10. T. Brabec and F. Krausz, "Intense few-cycle laser fields: Frontiers of nonlinear optics," Rev. Mod. Phys. **72**, 545–591 (2000).

#259068 Received 17 Feb 2016; revised 24 Mar 2016; accepted 29 Mar 2016; published 20 Apr 2016

11. M. T. Hassan, T. T. Luu, A. Moulet, O. Raskazovskaya, P. Zhokhov, M. Garg, N. Karpowicz, A. M. Zheltikov, V. Pervak, F. Krausz, and E. Goulielmakis, "Optical attosecond pulses and tracking the nonlinear response of bound electrons," Nature **530**, 66–70 (2016).
12. F. X. Kärtner, *Few-Cycle Laser Pulse Generation and Its Applications* (Springer, 2004).
13. S. Rausch, T. Binhammer, A. Harth, J. Kim, R. Ell, F. X. Kärtner, and U. Morgner, "Controlled waveforms on the single-cycle scale from a femtosecond oscillator," Opt. Express **16**, 9739–9745 (2008).
14. S. H. Cho, F. X. Kärtner, U. Morgner, E. P. Ippen, J. G. Fujimoto, J. E. Cunningham, and W. H. Knox, "Generation of 90-nJ pulses with a 4-MHz repetition-rate Kerr-lens mode-locked Ti:Al_2O_3 laser operating with net positive and negative intracavity dispersion," Opt. Lett. **26**, 560–562 (2001).
15. S. Naumov, A. Fernandez, R. Graf, P. Dombi, F. Krausz, and A. Apolonski, "Approaching the microjoule frontier with femtosecond laser oscillators," New J. Phys. **7**, 216 (2005).
16. H. Fattahi, H. G. Barros, M. Gorjan, T. Nubbemeyer, B. Alsaif, C. Y. Teisset, M. Schultze, S. Prinz, M. Haefner, M. Ueffing, A. Alismail, L. Vámos, A. Schwarz, O. Pronin, J. Brons, X. T. Geng, G. Arisholm, M. Ciappina, V. S. Yakovlev, D.-E. Kim, A. M. Azzeer, N. Karpowicz, D. Sutter, Z. Major, T. Metzger, and F. Krausz, "Third-generation femtosecond technology," Optica **1**, 45–63 (2014).
17. C. Gohle, T. Udem, M. Herrmann, J. Rauschenberger, R. Holzwarth, H. A. Schuessler, F. Krausz, and T. W. Hänsch, "A frequency comb in the extreme ultraviolet," Nature **436**, 234–237 (2005).
18. M. Krebs, S. Hadrich, S. Demmler, J. Rothhardt, A. Zair, L. Chipperfield, J. Limpert, and A. Tünnermann, "Towards isolated attosecond pulses at megahertz repetition rates," Nature Photon. **7**, 555–559 (2013).
19. Y. Liu, S. Tschuch, M. Dürr, A. Rudenko, R. Moshammer, J. Ullrich, M. Siegel, and U. Morgner, "Towards non-sequential double ionization of Ne and Ar using a femtosecond laser oscillator," Opt. Express **15**, 18103–18110 (2007).
20. A. Mikkelsen, J. Schwenke, T. Fordell, G. Luo, K. Klunder, E. Hilner, N. Anttu, A. A. Zakharov, E. Lundgren, J. Mauritsson, J. N. Andersen, H. Q. Xu, and A. L'Huillier, "Photoemission electron microscopy using extreme ultraviolet attosecond pulse trains," Rev. Sci. Instrum. **80**, 123703 (2009).
21. C. Jauregui, J. Limpert, and A. Tünnermann, "High-power fibre lasers," Nature Photon. **7**, 861–867 (2013).
22. P. Russbueldt, D. Hoffmann, M. Hofer, J. Lohring, J. Luttmann, A. Meissner, J. Weitenberg, M. Traub, T. Sartorius, D. Esser, R. Wester, P. Loosen, and R. Poprawe, "Innoslab amplifiers," IEEE J. Sel. Top. Quantum Electron. **21**, 447–463 (2015).
23. T. Metzger, M. Gorjan, M. Ueffing, C. Y. Teisset, M. Schultze, R. Bessing, M. Häfner, S. Prinz, D. Sutter, K. Michel, H. Barros, Z. Major, and F. Krausz, in *CLEO: Applications and Technology*, (Optical Society of America, 2014), p. JTh4L.1.
24. D. Bauer, I. Zawischa, D. H. Sutter, A. Killi, and T. Dekorsy, "Mode-locked Yb:YAG thin-disk oscillator with 41 μJ pulse energy at 145 W average infrared power and high power frequency conversion," Opt. Express **20**, 9698–9704 (2012).
25. C. J. Saraceno, F. Emaury, C. Schriber, M. Hoffmann, M. Golling, T. Südmeyer, and U. Keller, "Ultrafast thin-disk laser with 80μJ pulse energy and 242 W of average power," Opt. Lett. **39**, 9–12 (2014).
26. C. J. Saraceno, F. Emaury, O. H. Heckl, C. R. E. Baer, M. Hoffmann, C. Schriber, M. Golling, T. Südmeyer, and U. Keller, "275 W average output power from a femtosecond thin disk oscillator operated in a vacuum environment," Opt. Express **20**, 23535–23541 (2012).
27. J. Brons, V. Pervak, E. Fedulova, D. Bauer, D. Sutter, V. Kalashnikov, A. Apolonskiy, O. Pronin, and F. Krausz, "Energy scaling of Kerr-lens mode-locked thin-disk oscillators," Opt. Lett. **39**, 6442–6445 (2014).
28. J. Brons, V. Pervak, M. Seidel, D. Bauer, D. Sutter, O. Pronin, and F. Krausz, in *Advanced Solid State Lasers*, (Optical Society of America, 2015), p. ATh3A.1.
29. O. Pronin, M. Seidel, F. Lücking, J. Brons, E. Fedulova, M. Trubetskov, V. Pervak, A. Apolonski, T. Udem, and F. Krausz, "High-power multi-megahertz source of waveform-stabilized few-cycle light," Nat. Commun. **6**, 6988 (2015).
30. J. Zhang, J. Brons, M. Seidel, V. Pervak, V. Kalashnikov, Z. Wei, A. Apolonski, F. Krausz, and O. Pronin, in *The European Conference on Lasers and Electro-Optics* , (Optical Society of America, 2015), p. PDA.1.
31. W. H. Knox, R. L. Fork, M. C. Downer, R. H. Stolen, C. V. Shank, and J. A. Valdmanis, "Optical pulse compression to 8 fs at a 5 khz repetition rate," Appl. Phys. Lett. **46**, 1120–1121 (1985).
32. R. L. Fork, C. H. B. Cruz, P. C. Becker, and C. V. Shank, "Compression of optical pulses to six femtoseconds by using cubic phase compensation," Opt. Lett. **12**, 483–485 (1987).
33. T. Südmeyer, F. Brunner, E. Innerhofer, R. Paschotta, K. Furusawa, J. C. Baggett, T. M. Monro, D. J. Richardson, and U. Keller, "Nonlinear femtosecond pulse compression at high average power levels by use of a large-mode-area holey fiber," Opt. Lett. **28**, 1951–1953 (2003).
34. C. Jocher, T. Eidam, S. Hädrich, J. Limpert, and A. Tünnermann, "Sub 25 fs pulses from solid-core nonlinear compression stage at 250 W of average power," Opt. Lett. **37**, 4407–4409 (2012).
35. A. V. Smith, B. Do, G. Hadley, and R. L. Farrow, "Optical damage limits to pulse energy from fibers," IEEE J. Sel. Top. Quantum Electron. **15**, 153–158 (2009).
36. C. Rolland and P. B. Corkum, "Compression of high-power optical pulses," J. Opt. Soc. Am. B **5**, 641–647 (1988).

#259068 Received 17 Feb 2016; revised 24 Mar 2016; accepted 29 Mar 2016; published 20 Apr 2016

37. V. Petrov, W. Rudolph, and B. Wilhelmi, "Compression of high-energy femtosecond light pulses by self-phase modulation in bulk media," J. Mod. Opt. **36**, 587–595 (1989).
38. P. Chernev and V. Petrov, "Self-focusing of short light pulses in dispersive media," Opt. Commun. **87**, 28 – 32 (1992).
39. P. Chernev and V. Petrov, "Self-focusing of light pulses in the presence of normal group-velocity dispersion," Opt. Lett. **17**, 172–174 (1992).
40. N. Milosevic, G. Tempea, and T. Brabec, "Optical pulse compression: bulk media versus hollow waveguides," Opt. Lett. **25**, 672–674 (2000).
41. M. Nisoli, S. De Silvestri, and O. Svelto, "Generation of high energy 10 fs pulses by a new pulse compression technique," Appl. Phys. Lett. **68**, 2793–2795 (1996).
42. C.-H. Lu, Y.-J. Tsou, H.-Y. Chen, B.-H. Chen, Y.-C. Cheng, S.-D. Yang, M.-C. Chen, C.-C. Hsu, and A. H. Kung, "Generation of intense supercontinuum in condensed media," Optica **1**, 400–406 (2014).
43. J. C. Travers, W. Chang, J. Nold, N. Y. Joly, and P. S. J. Russell, "Ultrafast nonlinear optics in gas-filled hollow-core photonic crystal fibers (invited)," J. Opt. Soc. Am. B **28**, A11–A26 (2011).
44. F. Benabid, J. C. Knight, G. Antonopoulos, and P. S. J. Russell, "Stimulated raman scattering in hydrogen-filled hollow-core photonic crystal fiber," Science **298**, 399–402 (2002).
45. O. H. Heckl, C. J. Saraceno, C. R. E. Baer, T. Südmeyer, Y. Y. Wang, Y. Cheng, F. Benabid, and U. Keller, "Temporal pulse compression in a xenon-filled kagome-type hollow-core photonic crystal fiber at high average power," Opt. Express **19**, 19142–19149 (2011).
46. F. Emaury, C. J. Saraceno, B. Debord, D. Ghosh, A. Diebold, F. Gèrôme, T. Südmeyer, F. Benabid, and U. Keller, "Efficient spectral broadening in the 100-W average power regime using gas-filled Kagome HC-PCF and pulse compression," Opt. Lett. **39**, 6843–6846 (2014).
47. K. F. Mak, M. Seidel, O. Pronin, M. H. Frosz, A. Abdolvand, V. Pervak, A. Apolonski, F. Krausz, J. C. Travers, and P. S. J. Russell, "Compressing μJ-level pulses from 250 fs to sub-10 fs at 38-MHz repetition rate using two gas-filled hollow-core photonic crystal fiber stages," Opt. Lett. **40**, 1238–1241 (2015).
48. M. Gebhardt, C. Gaida, S. Hädrich, F. Stutzki, C. Jauregui, J. Limpert, and A. Tünnermann, "Nonlinear compression of an ultrashort-pulse thulium-based fiber laser to sub-70 fs in Kagome photonic crystal fiber," Opt. Lett. **40**, 2770–2773 (2015).
49. S. Hädrich, M. Krebs, A. Hoffmann, A. Klenke, J. Rothhardt, J. Limpert, and A. Tünnermann, "Exploring new avenues in high repetition rate table-top coherent extreme ultraviolet sources," Light Sci Appl **4**, e320 (2015).
50. M. Seidel, J. Brons, E. Fedulova, V. Pervak, A. Apolonski, O. Pronin, and F. Krausz, in *CLEO: Science and Innovations*, (Optical Society of America, 2014), p. STh5C.9.
51. P. M. W. French, "The generation of ultrashort laser pulses," Rep. Prog. Phys. **58**, 169 (1995).
52. R. W. Boyd, *Nonlinear Optics* (Academic 2008), Chap. 7.
53. A. Yariv, *Quantum Electronics* (John Wiley and Sons, Inc., 1989), Chap 18.
54. M. Centurion, M. A. Porter, P. G. Kevrekidis, and D. Psaltis, "Nonlinearity management in optics: Experiment, theory, and simulation," Phys. Rev. Lett. **97**, 033903 (2006).
55. O. Pronin, J. Brons, C. Grasse, V. Pervak, G. Boehm, M.-C. Amann, V. L. Kalashnikov, A. Apolonski, and F. Krausz, "High-power 200 fs Kerr-lens mode-locked Yb:YAG thin-disk oscillator," Opt. Lett. **36**, 4746–4748 (2011).
56. R. R. Alfano and S. L. Shapiro, "Emission in the region 4000 to 7000 å via four-photon coupling in glass," Phys. Rev. Lett. **24**, 584–587 (1970).
57. A. Couairon and A. Mysyrowicz, "Femtosecond filamentation in transparent media," Phys. Rep. **441**, 47 – 189 (2007).
58. M. Bradler, P. Baum, and E. Riedle, "Femtosecond continuum generation in bulk laser host materials with sub-μJ pump pulses," Appl. Phys. B **97**, 561–574 (2009).
59. Newport, "Spatial filters," http://www.newport.com/Spatial-Filters/144910/1033/content.aspx (2015/11/13).
60. G. Arisholm, "General numerical methods for simulating second-order nonlinear interactions in birefringent media," J. Opt. Soc. Am. B **14**, 2543–2549 (1997).
61. G. Arisholm, "Quantum noise initiation and macroscopic fluctuations in optical parametric oscillators," J. Opt. Soc. Am. B **16**, 117–127 (1999).
62. G. Ghosh, "Dispersion-equation coefficients for the refractive index and birefringence of calcite and quartz crystals," Opt. Commun. **163**, 95 – 102 (1999).
63. D. Milam, "Review and assessment of measured values of the nonlinear refractive-index coefficient of fused silica," Appl. Opt. **37**, 546–550 (1998).
64. N. Krebs, I. Pugliesi, and E. Riedle, "Pulse compression of ultrashort uv pulses by self-phase modulation in bulk material," Appl. Sci. **3**, 153 (2013).
65. U. Møller, Y. Yu, I. Kubat, C. R. Petersen, X. Gai, L. Brilland, D. Méchin, C. Caillaud, J. Troles, B. Luther-Davies, and O. Bang, "Multi-milliwatt mid-infrared supercontinuum generation in a suspended core chalcogenide fiber," Opt. Express **23**, 3282–3291 (2015).
66. F. Silva, D. R. Austin, A. Thai, M. Baudisch, M. Hemmer, D. Faccio, A. Couairon, and J. Biegert, "Multi-octave supercontinuum generation from mid-infrared filamentation in a bulk crystal," Nat. Commun. **3**, 807 (2012).

#259068 Received 17 Feb 2016; revised 24 Mar 2016; accepted 29 Mar 2016; published 20 Apr 2016

67. F. Emaury, A. Diebold, C. J. Saraceno, and U. Keller, "Compact extreme ultraviolet source at megahertz pulse repetition rate with a low-noise ultrafast thin-disk laser oscillator," Optica **2**, 980–984 (2015).
68. D. H. Reitze, A. M. Weiner, and D. E. Leaird, "High-power femtosecond optical pulse compression by using spatial solitons," Opt. Lett. **16**, 1409–1411 (1991).

1. Introduction

Ultrashort pulses have found a great variety of cutting-edge applications in science and technology, such as femtochemistry and -biology, laser micromachining, high-speed communication, metrology, or time-resolved spectroscopy in any type of matter [1–5]. For some applications, like attosecond metrology, ultrafast current switching in dielectrics or extreme ultraviolet high-harmonic spectroscopy of solids, pulse durations of only a few optical cycles are required [6–9]. This few-cycle regime can routinely be reached with amplifier systems [10] and could be even extended to durations on the sub-cycle level [11]. The utilized systems usually operate at high peak power (GW level) but low average powers ($<$ W) and repetition rates ($<$ 10 kHz), resp. At MHz repetition rates the broad gain bandwidth of Titanium doped sapphire (Ti:Sa) lasers has been exploited to generate few-cycle pulses [12, 13]. However, Ti:Sa oscillators can only be operated at several Watts of average power and sub-μJ pulse energies [14, 15]. Therefore, they are not suited for the next generation of femtosecond technology which targets upscaling of both average and peak power [16]. This would for instance enable XUV frequency comb spectroscopy without the need of complex enhancement cavities [17], high photon flux attosecond spectroscopy [18] and reaction microscopy as well as photoelectron emission microscopy at high data acquisition rates [19, 20].

Currently, three architectures compete for reaching new records in combining peak and average power. These are fiber [21], innoslab [22] and disk [16,23] technologies. Among them, particular attention shall be addressed to mode-locked thin-disk (TD) oscillators. They are nowadays able to generate pulses with several tens of μJ pulse energy [24, 25], average powers of more than 250 W [26, 27] and peak powers of more than 60 MW, even up to 145 MW with post compression [28] - all without any amplification. This has distinct advantages such as low complexity and thus high reliability of the systems as well as excellent noise performance [29]. Furthermore, the absence of gain narrowing enables the generation of pulses as short as the 9 nm bandwidth of Yb:YAG allows [28] or in extreme cases, even much shorter [30]. Nevertheless, direct few-cycle pulse generation from any power-scalable laser architecture is not in sight and hence external spectral broadening and pulse compression will be essential to reach the ultrashort pulse regime.

Historically, the first sub-10 fs pulses have been generated by means of spectral broadening in solid-core fiber and subsequent compression of the chirped pulses [31, 32]. This method was also successfully transferred to high power architectures, resulting in compression of pulses from a sub-ps TD oscillator mode-locked with a semiconductor saturable absorber mirror (SESAM) to about 30 fs [33], sub-20 fs from a Kerr-lens mode-locked (KLM) TD oscillator [29] and sub-25 fs pulses at 250 W of average power from a fiber amplifier system [34]. However, despite the average power scalability of the concept, it is hardly peak power scalable due to the onset of critical self-focusing [35]. With the advent of chirped pulse amplification, peak power scalable spectral broadening became also a topic of intense research [10]. Rolland and Corkum proposed perhaps the simplest broadening technique which is focusing intense light into a bulk plate such that the critical self-focusing length exceeds the physical length of the nonlinear medium [36]. Although the study accomplished a pulse compression from 92 fs to 19 fs and was followed by several theoretical papers discussing the method [37–39], the power efficiency of only about 4 % made the method fairly unattractive. In 2000, Milosevic et al. explicitly evaluated the strengths and weaknesses of pulse compression in bulk media in comparison to hollow core capillaries which have been applied to compress GW

#259068 Received 17 Feb 2016; revised 24 Mar 2016; accepted 29 Mar 2016; published 20 Apr 2016

peak power pulses for more than 20 years by now [10, 40, 41]. They employed coupled-mode theory to analyze the spatial losses in both techniques and found that broadening in solid material can only be made efficient if the peak power is much lower than the critical power of the material. This claim, which refers to single-plate broadening, has become questionable owing to the findings of Lu et al. [42] who efficiently broadened ultrashort pulses with GW peak power level.

With respect to the latest generation of high-power fs sources, the applicability of capillaries is fairly limited since the transmission losses of waveguides with less than 100 μm core diameter are huge [43]. But fairly small diameters are required to generate sufficient nonlinear effects for pulses with MW-level peak powers. An alternative approach for spectral broadening in this range is the use of hollow-core photonic crystal fibers (HC-PCF) with a kagomé-lattice cladding structure [43, 44]. Among other things, this technique has been utilized for pulse compression with high-power TD oscillators [45–47] and fiber amplifiers [48, 49].

Nevertheless, the studies in our laboratories discouraged us from continuing to use gas-filled HC-PCFs for pulse compression. Despite reaching the few-cycle regime at 18 W average power [47], several distinct disadvantages of the technology became apparent. Firstly, plasma build-up was observed in xenon and krypton gases despite staying clearly below the ionization threshold of the gases. This forced us to apply a pressure gradient in the fiber. Secondly, even after avoiding ionization, the intensity noise was significantly raised after the first and the second stage and appeared to be highly sensitive to the coupling. Thirdly, the fiber coupling was time-consuming and had to be optimized frequently. Spectral broadening in bulk material, which has also allowed few-cycle pulse generation from a thin-disk oscillator [29, 50], circumvents all these issues. It comes with low complexity and costs, is highly robust and exhibits excellent noise properties. In order to realize any of the applications mentioned above, a reliable and easy-to-handle technology is imperative [51]. This study will show that bulk broadening fulfills these requirements. Moreover, peak and average power scalability of the method will be illuminated.

The manuscript is structured as follows: First, the parameters which have impact on the broadening performance are discussed qualitatively. An experimental study of these parameters is presented afterwards. Subsequently, the broadened spectra and spectral phases are analyzed. An example of cascaded bulk broadening with intermediate compression follows. Next, the losses due to the coupling of spectral and spatial nonlinear effects are investigated. The experimental part is completed by a check of the noise properties of the spectrally broadened pulses. A simulation section follows which investigates the power scalability of the concept. Finally, all results are summarized and conclusions on the applicability of bulk broadening are drawn.

2. General aspects of bulk broadening

In the absence of significant dispersion and divergence the critical power (P_{cr}) of a nonlinear medium is approximately [52]:

$$P_{cr} = \frac{\pi(0.61)^2\lambda^2}{8n_0n_2}, \tag{1}$$

where λ is the vacuum wavelength, n_0 the linear and n_2 the nonlinear refractive index. Spectral broadening in bulk material is not limited by the critical power. The beam collapse can be avoided if the length of the medium is smaller than the critical self-focusing length z_{sf} which is approximately [52, 53]:

$$z_{sf} = \frac{\pi d^2}{\lambda\left(\sqrt{P_p/P_{cr}-1}-\theta\right)}, \tag{2}$$

#259068 Received 17 Feb 2016; revised 24 Mar 2016; accepted 29 Mar 2016; published 20 Apr 2016

where d is the beam diameter at the input facet of the medium, P_p the peak power of the laser pulses and θ the beam divergence. Assuming a 1 μm wavelength, the maximal critical power for solid materials is approximately 8 MW (for CaF_2) and thus far below the peak powers of amplifier systems or the latest mode-locked TD oscillators. Therefore, to avoid critical self-focusing, either the beam diameter has to be expanded or the beam divergence has to be adapted to counteract the focusing effect.

To visualize these approaches Fig. 1(a) shows how the peak irradiance evolves in three exemplary studies. The green dashed line represents the propagation of a 1.2 μJ, 250 fs pulse through 15 mm of crystalline quartz. All pulse durations and Fourier transform limits (FTLs) stated in the text refer to the full width at half maximum (FWHM) of a pulse. The peak power ($P_p = 4.2$ MW) is slightly above the critical power of the material ($P_{cr} \approx 3.6$ MW). The divergence is set to zero at the front facet of the nonlinear material. In order to stay below the critical irradiance (2 TW/cm^2 assumed) the input peak irradiance must not be larger than 180 GW/cm^2. For a 10 μJ, 250 fs pulse ($P_p = 35.2$ MW, red line) the input peak irradiance has to be even smaller (110 GW/cm^2) in order to avoid damage of the nonlinear material. This is due to the highly nonlinear beam divergence induced by the strong self-focusing inside the material. The behavior is not covered in the derivation of Eq. (2) in [53]. It expands the beam area in terms of the peak irradiance and truncates the expansion after the linear term which leads to the wrong statement that the peak irradiance at the entrance facet of the nonlinear material can be raised with increasing peak power of the input pulses if plate thickness and beam divergence are fixed. However, Eq. (2) predicts correctly that the peak irradiance at the entrance facet of a nonlinear material, and thus self-phase modulation (SPM), can be increased by strongly focusing the laser beam in order to apply a high (Gaussian) beam divergence. Fig. 1(a) shows that the b-integral (i.e. the area under a curve) of the initially divergent beam (blue line) is higher than that of a

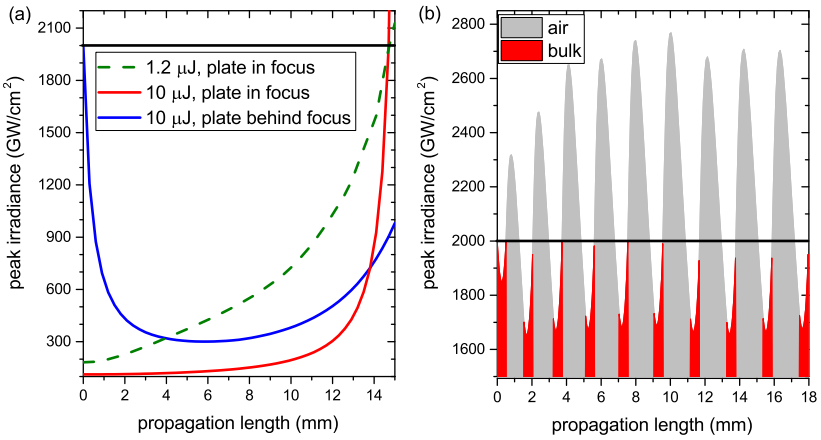

Fig. 1. Means of avoiding critical self-focusing within a nonlinear crystal. The plots are taken from simulations which are explained in more detail in section 4. A peak irradiance of 2 TW/cm^2 is considered as critical (solid black line markers). (a) Single plate approach: critical self-focusing is avoided by choosing a large spot size at the entrance facet (dashed green line: 1.2 μJ, 250 fs input pulses, $d = 77\,\mu$m; red line: 10 μJ, 250 fs input pulses, $d = 283\,\mu$m) or by utilizing a strong beam divergence to compensate for self-focusing (blue line: 10 μJ, 250 fs input pulses, $d = 67\,\mu$m, $\theta = 32\,\mu$m/mm). (b) Multiple plate approach: The beam irradiance is kept below the critical value inside the solid medium while the foci lie in the air gaps between the thin bulk plates (10 μJ, 250 fs input pulses).

#259068 Received 17 Feb 2016; revised 24 Mar 2016; accepted 29 Mar 2016; published 20 Apr 2016

beam where $\theta = 0$ (red line). Nevertheless, the area under the green dashed line (1.2 μJ, 250 fs pulses) is the largest and thus the strongest spectral broadening is anticipated in this case.

Ideally, a spectral broadening experiment induces as much SPM as possible while the nonlinear distortions of the beam, caused by self-focusing, are kept as low as possible. However, without additional beam shaping or guiding, the spatial and temporal nonlinearities cannot be decoupled [40]. A promising self-guiding mechanism relies on a sequence of thin plates which are arranged such that the laser beam alternatingly focuses and defocuses [54]. Air has a critical power of $P_{cr} \approx 5$ GW at 1030 nm [57] and thus exhibits negligible self-focusing at the considered peak power levels. Multi-photon ionization is expected to become relevant at intensities of about 10^{13} W/cm^2 [57]. The principle of alternating bulk and air sequences was recently exploited to avoid multiple filaments in white-light continuum (WLC) generation which led to a strong suppression of spatial losses in the spectral broadening experiment [42]. This multi-plate approach will be studied numerically in order to evaluate if it can be transferred to longer initial pulse durations than in the original publication and MW level peak powers which are common in the latest generation of high power MHz laser systems. The evolution of the peak irradiance is compared to the single plate approach in Fig. 1(b). The graph shows a sequence of ten 0.5 mm thick quartz plates. The incident pulse has a duration of 250 fs and 10 μJ energy. The variations of the peak irradiance is much smaller than in the single plate examples. Moreover, the beam is always focused in between the bulk plates. The examples of Fig. 1 will be analyzed in detail in the simulation section of the manuscript and shall give for now only basic insights into the beam behavior in the nonlinear sample.

3. Experiment

3.1. Spectral broadening under variation of focal length and material

In the experiments a Kerr-lens mode-locked TD oscillator was utilized which delivered an average power of 50 W at a repetition rate of 38 MHz. This corresponds to 1.3 μJ pulse energy. The initial pulse duration is 250 fs and the central wavelength $\lambda = 1.03\,\mu$m. Details of the oscillator are described in [55]. The experimental setup is shown in Fig. 2.

Several wide band gap materials were tested. Crystalline quartz performed better than fused silica due to its higher thermal conductivity. Sapphire yielded broadening factors similar to quartz. A YAG crystal was damaged before significant broadening set in. This could be at-

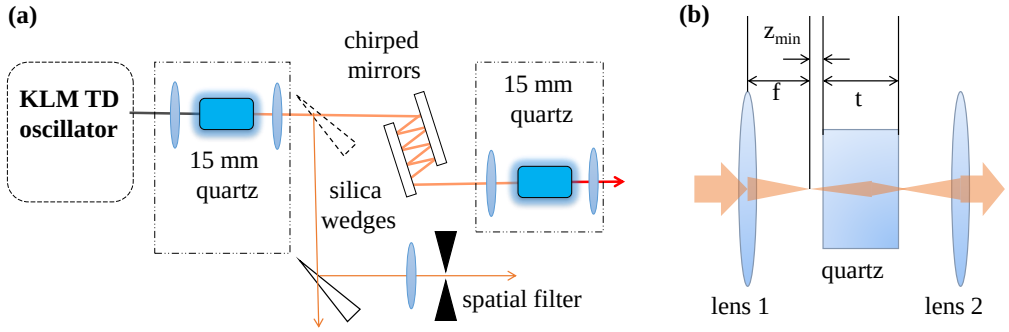

Fig. 2. Setup of the bulk broadening experiments. (a) Overview of all performed experiments. The wedge sketched by a dashed line was inserted for characterization purposes and was not present during the compression experiments. (b) Detailed sketch of the spectral broadening stages symbolized by the dotted-dashed lines in (a). The characteristic lengths t, f and z_{min} were varied for optimization purposes.

#259068 Received 17 Feb 2016; revised 24 Mar 2016; accepted 29 Mar 2016; published 20 Apr 2016

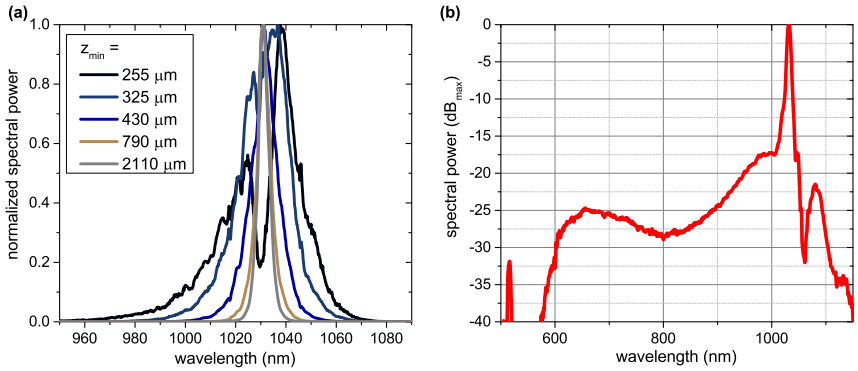

Fig. 3. (a) Spectra measured with an OSA in dependence on z_{min}. The focal length was f = 25 mm. The spectrum was filtered such that only the broadened parts were measured. (b) White-light continuum generated in a 15 mm quartz crystal. The spike at 515 nm is the second harmonic generated in the quartz crystal due to its $\chi^{(2)}$-nonlinearity.

tributed to impurities in the material which were indicated by a violet glow not observable in the other materials. Additionally, several crystal lengths were tested. Best spectral broadening results could be achieved with quartz and sapphire crystals of at least t = 6 mm thickness. Eventually, a 15 mm thick quartz crystal was chosen in the experiments.

To adjust the broadening factor, i.e. the FTL ratio between incoming and outgoing pulses, the sample was slowly moved towards the focus position of lens 1 while the spectrum was monitored after lens 2 with an optical spectrum analyzer (OSA). The obtained spectra are shown in Fig. 3(a). The focal lengths f were varied from 18 mm to 100 mm. The maximal achievable broadening was not very sensitive to the variation. The location of damage inside the crystal shifted however if z_{min} was set too small. This is explained by the critical irradiance where ionization sets in. It is reached at the entrance facet if the beam is focused strongly while it is observed inside the crystal if focusing is loose and the self-focusing leads to a beam collapse.

Longer focal lengths also allowed white-light continuum generation [56,57]. The continuum is shown in Fig. 3(b). However, ionization, which is essential for WLC generation, was avoided in all other presented experiments. This was because firstly, the WLC was rather unstable and a noticeable heating of the crystal occurred. Therefore, average power scalability of the approach requires strong technical efforts. Secondly, the prominent blue shoulder is 25 dB below the fundamental and thus the conversion into the continuum is fairly weak ($< 20\,\%$). Thirdly, WLC generation depends on the input pulse duration and gets rather difficult for longer pulses [58]. No ionization losses were detected by means of power measurements for the spectra displayed in Fig. 3(a). The spectral broadening is caused solely by SPM.

In this case, the Fourier transform limit of the pulses could be reduced from 250 fs to 38 fs (black solid line Fig. 3(a)). This corresponds to a broadening factor of about 6 which is the largest in a single-stage bulk broadening experiment to the best of the authors' knowledge.

3.2. *Temporal phase behavior under variation of broadening strength*

In order to compress the spectrally broadened pulses, the evolution of the spectral phase under variation of the distance from the focus to the crystal facet (z_{min}) was measured by means of second harmonic frequency resolved optical gating (SH-FROG). The SH-FROG did not contain any dispersive elements apart from the SH crystal. The beam splitting was done through wavefront division by means of a D-shaped silver mirror. A 5 μm BBO was used as a nonlinear crystal. Fig. 4(a) shows the calculated FTL as well as the peak power ratio between pulses with

#259068 Received 17 Feb 2016; revised 24 Mar 2016; accepted 29 Mar 2016; published 20 Apr 2016

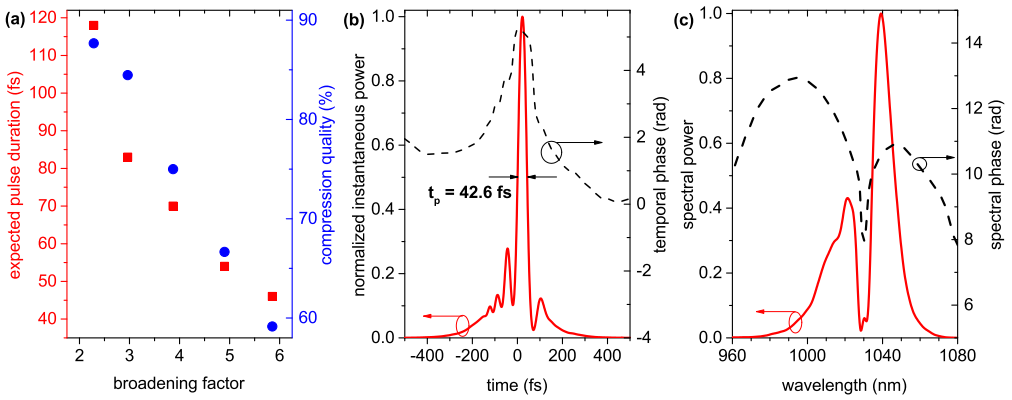

Fig. 4. (a) Expected pulse durations in dependence on the broadening factor for compensation of first order chirp only (red squares). The compression quality (blue circles) is the ratio between the peak power of the compressed and the Fourier limited pulse. (b) Retrieved pulse after compressor. The compression quality is 64 % (c) retrieved spectrum and spectral phase. The spectrum is in good agreement with the black line in Fig. 3(a).

first order chirp compensation only and transform limited pulses. The quantity is denoted by compression quality. Compensating higher order phase terms, for instance by a tailored chirped mirror design, would lead to shorter pulses and less power in the pedestals [29].

The chirped mirror compressor was set up such that shortest pulses could be achieved. A GDD of -1700 fs^2 was predicted and realized by 4 bounces off mirrors with -400 fs^2 GDD and no higher order terms. A pulse duration of 43 fs was measured. It is in good agreement with the predicted pulse duration of 46 fs for a slightly more negative GDD. The pulse in Fig. 4(b) shows a significant pedestal structure carrying about 35 % total energy which agrees with the prediction in Fig. 4(a). Larger broadening factors come also with an increase of spatial losses due to the coupling of self-focusing and SPM. This has not been considered in this section but will be addressed in detail in the simulation part of this work.

3.3. *Cascading bulk broadening with intermediate compression*

In our previous experiments on high-power bulk broadening, 17 fs input pulses were broadened and compressed down to 7.7 fs [29]. To bridge the gap from the experiments reported here to [29], a second bulk broadening stage was set up. After a first bulk stage, the pulses were compressed to 53 fs duration with a total GDD of -2400 fs^2 and afterwards focused with an anti-reflection coated lens (f = 35 mm) into another 15 mm quartz crystal (Fig. 2(a)). After optimizing z_{min}, the FTL could be reduced to 15 fs (Fig. 5). The modulations of the spectral power arise from the pedestal structure of the pulse after the first compression stage. The increase in bandwidth of the second stage is clearly larger than in the first stage. This is due to the steeper temporal gradient of the pulse. The broadening factor is about 3.5. The decrease in comparison to the first stage can be attributed to the increasing impact of dispersion. It should be pointed out that the achieved Fourier transform limit is comparable to the one which was obtained by fiber compression in [29] and hence there is strong evidence that all-bulk broadening enables few-cycle pulse generation at peak power levels way beyond the material's critical power.

3.4. *Spatial characterization*

Owing to the free beam propagation within the bulk material, temporal and spatial nonlinear effects are coupled and have to be taken into account when the efficiency of the compression stage

#259068 Received 17 Feb 2016; revised 24 Mar 2016; accepted 29 Mar 2016; published 20 Apr 2016

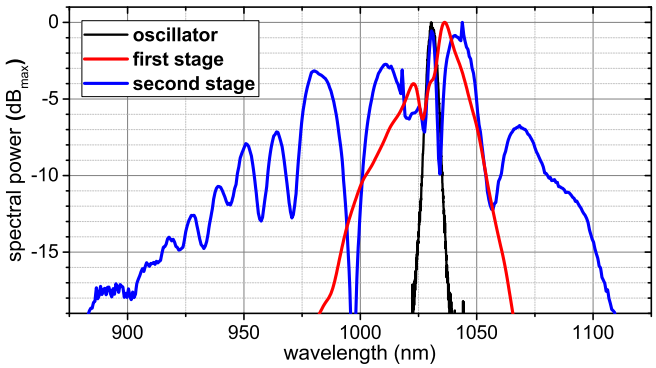

Fig. 5. Double stage spectral broadening. The FTL is reduced from 250 fs to 15 fs after the second stage.

is calculated. While strong SPM will lead to broad spectra in the beam center, i.e. in the region of high irradiance, the FTL of the beam wings will hardly be changed since the irradiance is too low. The spectrally filtered beam profiles shown in Fig. 6(a) have clearly different shapes. The broadened spectral parts (around 1010 nm and 1050 nm) exhibit more desirable Gaussian shapes in contrast to the unbroadened spectral part around 1030 nm where a ring structure is visible. Therefore, measuring the spectrum emerging from the nonlinear crystal became position sensitive.

In order to spectrally homogenize the beam and to estimate the losses due to spatial nonlinearities, a spatial filtering experiment was set up. It was performed with about 100 mW average power, reflected from two wedges (Fig. 2(a)). A 10 μm pinhole was used and the best focal lengths of the lenses in front of the pinhole (f_p) were calculated by [59]:

$$f_p = \frac{w_0 d_p}{\lambda}, \tag{3}$$

where w_0 is the waist of the collimated beam and d_p is the pinhole diameter.

First, the unbroadened, collimated oscillator output (M^2 = 1.05) was sent through the pinhole to verify the spatial filter performance, yielding 87 % transmission of the incident power. Afterwards, the 1010 nm bandpass was inserted into the broadened beam and the lens 2 was adjusted to collimate the wings of the spectrum. After removing the bandpass, the spatial filtering experiment was repeated. A 53 % transmission of the total power was measured which is 40 % less than in the unbroadened case. This is considered as the power loss due to the spatial nonlinear effects. The spectrum behind the pinhole had a FTL of 40 fs. The homogeneity was proven by scanning the expanding beam after the pinhole with a multimode fiber coupled to the OSA. Moreover, an M^2 measurement of the spectrally broadened beam was performed according to ISO Standard 11146. It yielded $M^2 < 1.1$ along both space axes.

The spectrum after the pinhole is similar to the FROG spectrum. Due to the chromatic longitudinal shift of the focus position, the FROG acts like a spatial filter as well. Within the 5 μm thin BBO crystal only the spectrally broadened beam is in focus and thus generates a second harmonic signal. The retrieved FROG spectrum (Fig. 4(d)) shows a strong suppression of the 1030 nm component. The scattering light spectrum (Fig. 6(b)) can be decomposed into the part retrieved from the FROG measurement and the initial oscillator output, i.e. the spectral content of the rings at 1030 nm.

#259068 Received 17 Feb 2016; revised 24 Mar 2016; accepted 29 Mar 2016; published 20 Apr 2016

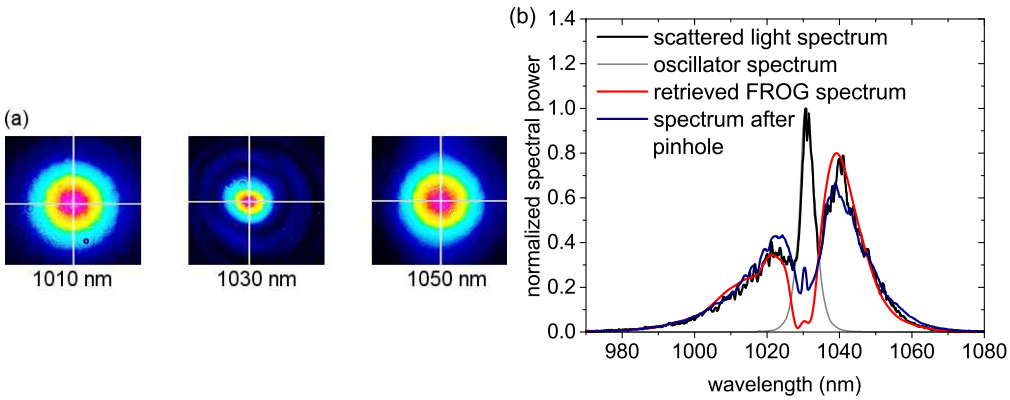

Fig. 6. Spatiotemporal effects of bulk broadening. (a) Beam profiles measured behind optical bandpass filters of 10 nm spectral width. The profiles behind the filters centered at 1010 nm (left) and 1050 nm (right) are Gaussian while the profile after the 1030 nm filter (center) exhibits a ring structure. The profiles were measured about 20 cm behind the collimation lens. (b) The scattered light spectrum (i.e. spatially integrated spectrum, black line), the retrieved FROG spectrum (red line) and the initial oscillator spectrum (gray line). The blue solid line shows the spectrum measured after spatial filtering.

3.5. Noise properties

Despite the fact that utilizing kagomé-type HC-PCFs for the compression of the oscillator pulses yielded sub-10 fs pulses in a double-stage setup [47], the applicability of the technique appeared to be restricted owing to the intensity noise accumulation in the broadening stages. Similar power fluctuation measurements were performed after the first bulk broadening stage, i.e. a small fraction of the laser beam was sent onto a fast photo diode to measure the power fluctuations of the pulse train. Fig. 7 shows that the accumulated intensity noise is independent of the position z_{min} and thus also independent of the broadening factor.

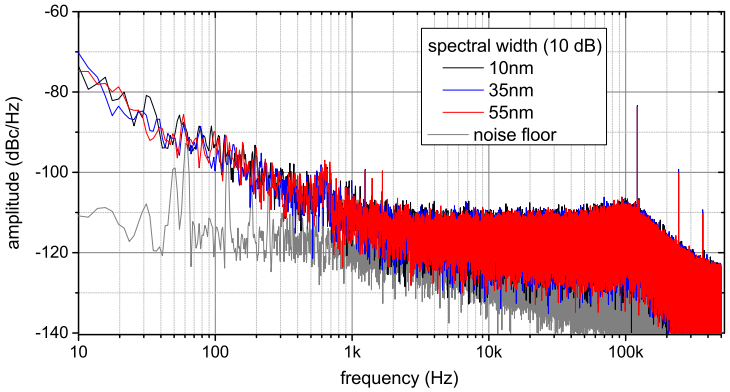

Fig. 7. Intensity noise measurements after the first bulk broadening stage for different broadening factors. The 55 nm spectral full width at -10 dB of the maximum corresponds to the black line in Fig. 3(a). The excellent noise properties of the oscillator (0.1 % rms relative intensity noise in the bandwidth from 10 Hz to 500 kHz) are maintained independent of the broadening factor.

#259068 Received 17 Feb 2016; revised 24 Mar 2016; accepted 29 Mar 2016; published 20 Apr 2016

4. Simulations

Full three-dimensional simulations of nonlinear pulse propagation [60,61] have been performed to address the question of power-scalability of the bulk broadening approach. The spatial grid is set to 513 x 513 points in a quarter of the x-y-plane which is justified by the fairly weak birefringence of quartz and the circular symmetry of the beams. The spacing is set to 10 points within the minimal $1/e^2$-radius. The temporal grid consists of 256 points with a 10 fs spacing. Simulations were done with the material dispersion derived from the crystalline quartz Sellmeier equation [62] and a nonlinear refractive index of $2.8 \times 10^{-16}\,\mathrm{cm}^2/\mathrm{W}$, taken from fused quartz [63]. The beam was treated as collapsed when a critical value of $2\,\mathrm{TW/cm}^2$ was reached inside the nonlinear crystal. In this case, the simulation was stopped and rerun with a larger input beam diameter or divergence. A first routine (i) set the front facet of the crystal into the focus and increased the spot size until no collapse occurred (solid red and dashed dark green lines Fig. 1(a)). A second routine (ii) set the peak irradiance on the front facet slightly below the damage threshold and increased divergence until the beam collapse was avoided (blue line Fig. 1(a)). The waist size, which was the optimization parameter in both routines, was varied in steps of $0.1\,\mu$m.

To benchmark the utilized code, the experimental parameters were used as the simulation input, i.e. a 250 fs, $1.2\,\mu$J pulse was focused into a 15 mm sample. Fig. 8 shows simulated spectra and profiles. Near-field profiles were extracted from the simulations while the experimental profiles (Fig. 6) were taken after tens of cm propagation. Qualitatively, the agreement of experiment and simulation is very good. The spectra show the asymmetry with a broader but less powerful blue shoulder. The spectra can be also decomposed into an unbroadened and a broadened part. The 1030 nm profile shows the ring structure while the 1040 nm profile looks Gaussian. The lowest achievable FTL is 31 fs. The broadening hardly depends on the focus spot size (i.e. focal length in the experiment) because the pulse peak power is close to the critical power of the material and thus the nonlinear lens is relatively weak. This is also in good agreement with the experimental observations. Therefore, it is inferred that the utilized code is suited to investigate the power-scalability of the bulk broadening approach.

Subsequently, the simulation was repeated with a $10\,\mu$J pulse, leaving all other input parameters unchanged. Hence, the critical power is exceeded by about an order of magnitude. Fig. 1(a) shows the evolution of the peak irradiance over the propagation distance derived from the rou-

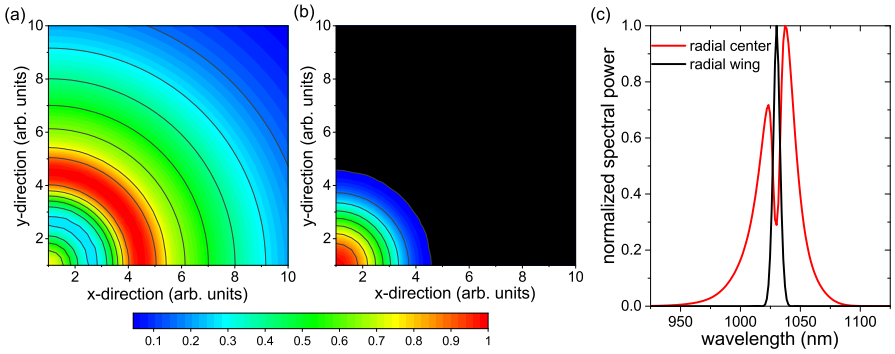

Fig. 8. Simulation of the spectral broadening in a 15 mm crystalline quartz crystal. (a) Near-field pattern of the 1030 nm filtered beam profile. (b) Near-field pattern of the 1040 nm filtered beam profile. (c) Radially dependent spectra, the black line shows the spectrum of the unbroadened part located in the wing of the near field-profile, th e red line shows the broadened spectrum located in the center of the near-field profile.

#259068 Received 17 Feb 2016; revised 24 Mar 2016; accepted 29 Mar 2016; published 20 Apr 2016

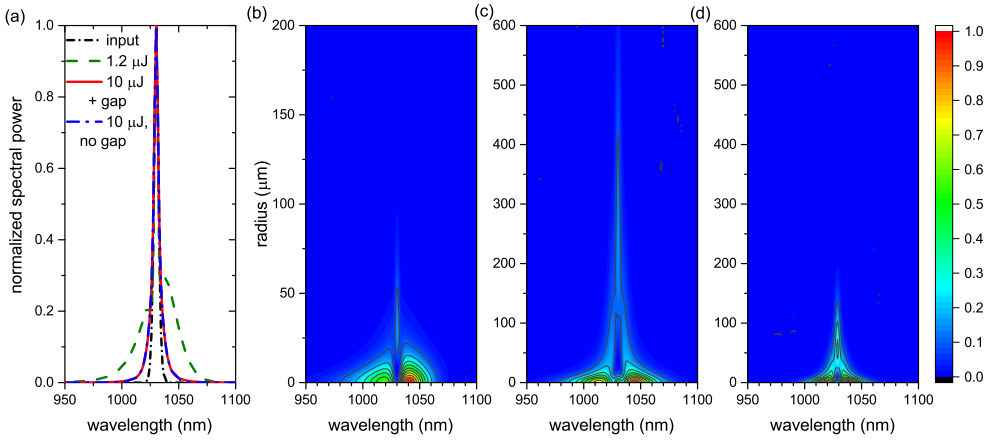

Fig. 9. Spatially integrated and radially resolved spectra after propagation through a 15 mm quartz plate. (a) Normalized spectra for (b) - (d) and the oscillator spectrum. The spectral power is integrated over the whole beam area. (b) 1.2 μJ, 250 fs input pulses. A significant part of the input beam is broadened like it was observed in the experiment. (c) 10 μJ, 250 fs input pulses with balanced divergence and self-focusing. The broadening in the beam center is comparable to (b) but only a small fraction ($\approx 4\,\%$) of the input power is broadened. (d) 10 μJ, 250 fs input pulses without divergence. The spectral broadening is weaker than in (b) and (c). About 16 % of the total power are contained in the broadened part. All color plots are scaled linearly and normalized. The units of the radially resolved spectra are J/Hz/μm^2, i.e. the pulse energies E are predicted by $E = 2\pi\Delta\nu\Delta r\sum_{i,j} r_i u(r_i, \nu_j)$, where $\Delta\nu$ and Δr are the simulation grid spacing in frequency and space, r is the radius and u is the plotted energy density. Is is summed over all spatial grid points r_i along one axis and all spectral grid points ν_j.

tines (i) and (ii). Moreover, the output spectra have been depicted in Fig. 9(a). The broadening seems much weaker than in the case of the 1.2 μJ input. This agrees well with experimental observations [28]. Nevertheless, the computed FTLs are 73 fs for routine (i) and 51 fs for routine (ii). The spatially resolved spectra (Fig. 9(b)-(d)) reveal that the central parts of the beam are still significantly broadened but they only contain a small amount of the pulse energy in comparison to the 1.2 μJ case. This shows that balancing divergence and self-focusing increases the broadening factor but also leads to a strong spectral inhomogeneity of the beam. Routine (ii) with 10 μJ pulses was repeated for 10 mm, 5 mm as well as 3 mm plates. The FTLs are 62 fs, 77 fs and 87 fs, resp. while the spectrally broadened parts amount 8 %, 15 % and 18 % of the total input power.

These observations suggest to apply the multiple-plate method which was demonstrated in [42] for spectral broadening of 25 fs pulses with hundreds of MW peak power. It is suspected that a similar method is mentioned in [22] for several hundred Watts of average power. Instead of using multiple plates, the focus behind a single plate (cf. Fig. 1(b)) can be self-imaged such that a virtual multiple-plate pattern is created. The experiment is however only scarcely described which makes its evaluation difficult. It is in any case remarkable that [22, 42] report fairly small spatial losses although the peak powers lie well above the critical powers of fused silica.

Therefore, another simulation algorithm was written. The simulation of the first plate is done with optimization routine (ii). The simulation of propagation through an air gap follows. The next plate is then set behind the focus in the air gap where the peak irradiance is below the critical value. If the beam collapses in the plate, the length of the air gap is extended. A sequence

#259068 Received 17 Feb 2016; revised 24 Mar 2016; accepted 29 Mar 2016; published 20 Apr 2016

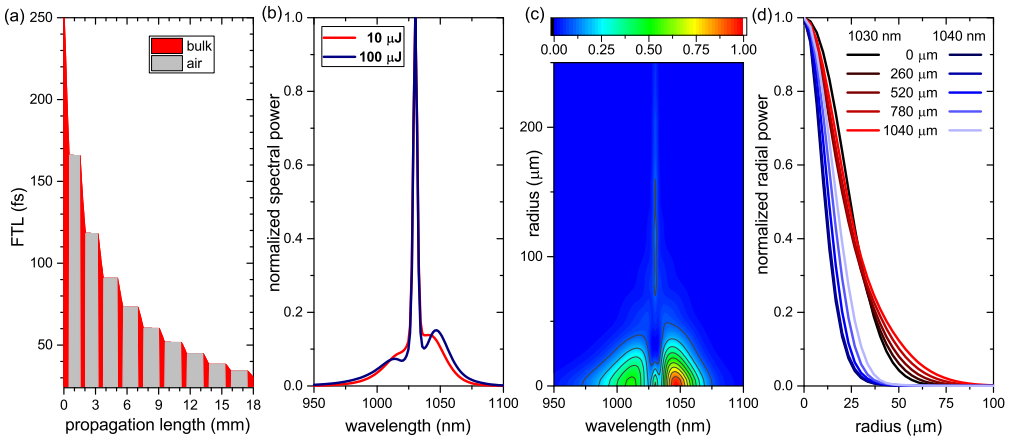

Fig. 10. Simulation of propagation of a 10 μJ pulse through ten 0.5 mm plates. No Fresnel losses are considered. (a) The FTL is inversely proportional to the plate number. The FTL after 10 plates is 31 fs. (b) The spatially integrated output spectrum after ten plates (red solid line). For comparison, the output spectrum of propagating a 100 μJ, 250 fs pulse through ten plates (solid blue line) (c) The spatially resolved output spectrum after 10 plates. (d) Spectrally resolved beam profiles for 1030 nm and 1040 nm during propagation in the first air gap (FTL = 165 fs). The broadened part emerging from the beam center (bluish lines) diverges quickly while the unbroadened part (reddish lines) is focused first and diverges slowly afterwards. The propagation length inside the gap is stated in the plot legend.

of ten 0.5 mm thick plates was simulated for a 10 μJ, 250 fs input pulse. The evolution of the peak irradiance along the plate assembly is shown in Fig. 1(b).

The simulation reveals a linear increase of bandwidth per plate. The FTL is inversely proportional to it which is shown in Fig. 10(a). Intermediate compression after a few plates would increase the slope dI(t)/dt and would thus lead to a stronger increase in bandwidth per plate. Experimentally, this behavior is indicated in Fig. 5. The most remarkable effect of the multiple-plate propagation is that the integrated spectrum resembles the one which was achieved with the 1.2 μJ pulses. Hence, a significant reduction of the spatial losses in comparison to the single plate approach could be achieved. This is demonstrated in Fig. 10(b) and (c). While the broadened parts of the single plate example (Fig. 9(c)) amount only 4 % of the total power, about 40 % are broadened in the multi-plate example. This can be attributed to the homogenizing effect of the air gaps which is visible in Fig. 10(d). The central, broadened parts diverge faster than the unbroadened parts in the wings of the beam. Hence, the unbroadened parts move to the most intense region of the beam and get broadened as well. The multi-plate routine was also executed with 100 μJ pulses (no other input parameters were changed). Fig. 10(b) shows an integrated spectrum similar to one with 10 μJ input pulses, i.e. the losses do not significantly differ. Furthermore, the 10 μJ pulse energy simulations were repeated with 0.2 mm thick plates. After ten plates, the FTL was 68 fs, the efficiency about 51 %. After 20 plates, the FTL was 35 fs and the efficiency about 44 %. Consequently, thinner plates do not necessarily yield better broadening performance. Determining the ideal plate thicknesses is subject of ongoing research. This work mainly points out the power scalability of the bulk broadening concept to peak power levels far beyond the critical power. The results for 1.2 μJ and 10 μJ pulses are summarized again in Table 1.

Eventually, the broadening in a single 0.5 mm plate was investigated. Routine (ii) was repeated with a constant peak power of 40 MW and with input pulse durations of 1 ps, 500 fs, 250 fs, 125 fs, 68 fs, 34 fs, 19 fs, and 9 fs. The temporal grid spacing was adapted corre-

#259068 Received 17 Feb 2016; revised 24 Mar 2016; accepted 29 Mar 2016; published 20 Apr 2016

Table 1: Summary of FTLs and Spatial Losses[a]

pulse energy (μJ)	1.2	1.2	10	10	10
routine	experiment	(i)	(i)	(ii)	(iii)
number of plates	1	1	1	1	10
plate thickness (mm)	15	15	15	15	0.5
FTL (fs)	38	31	73	51	31
estimated spatial losses (%)	40	60	84	96	60

[a]The input pulse duration is 250 fs and the nonlinear material is quartz. The routines are explained in the main text.

spondingly. All simulations yielded a broadening factor of about 1.5. Next, simulations with 250 fs input pulse duration and pulse energies of 1 μJ, 3 μJ, 5 μJ, 10 μJ, 30 μJ, 50 μJ, 100 μJ, 300 μJ, 500 μJ and 1 mJ were executed. Also in this study a broadening factor of about 1.5 was always found. It is inferred that purely SPM based bulk broadening is applicable to a wide range of input pulse durations and energies if the focus sizes and the plate positions are chosen appropriately.

5. Discussion

The single stage broadening led to an unprecedented high broadening and compression factor (about 6) and exhibited a much higher efficiency (about 60 %) than the initial experiments of Rolland and Corkum (compression factor about 5, efficiency about 4 %) [36]. It was shown that a single plate experiment, where the peak power exceeds the critical power, presents a trade-off between efficiency and broadening factor. This agrees with the results of the coupled-mode theory [10,40]. Additionally, it was found that higher broadening factors come at the expense of compression quality if no tailored chirped mirrors are available. In the presented experiments, the peak power of the pulses was increased from 4.2 MW to 9.5 MW. With tailored mirrors a peak power of 15 MW would be possible. Similar peak power enhancements of about a factor three could be reached with the simulated multi-plate compression scheme for 10 μJ pulses.

The single plate experiment is particularly attractive if only a small broadening factor (≈ 2) is targeted, for instance to reach the few-cycle regime [29]. Moreover, transferring the approach to other wavelengths is highly interesting. Krebs et al. performed for example experiments in the UV at kHz repetition rates [64]. Transferring the experiment to MHz rates would require peak irradiances lower than 2 TW/cm^2 to avoid ionization but is expected to be also possible due to the increased n_2 at shorter wavelengths. The bandgap of CaF_2 is about 12 eV, corresponding to a two-photon absorption edge of about 200 nm. This is expected to be the shortest wavelength where bulk broadening is possible. Similarly, the technique can be employed in the mid-IR range where silica fibers are not applicable at all due to the limited transparency range of quartz and soft glass fibers are limited to mW-level average power handling [65]. Huge broadening factors have been already achieved by means of filamentation in a YAG crystal at about 1 W average power [66].

If high-power pulse compression by means of kagomé-type lattice HC-PCFs and the bulk technique are compared, both methods show distinct advantages. The experimentally achieved transmission efficiencies in fiber (88% in [46]) are higher than the presented one in bulk (60%). HC-PCFs enable soliton self-compression in the anomalous dispersion regime [47] and higher compression factors in a single stage (11 in [47]). On the other hand, the relative intensity noise is increased by a factor of 1.6 (100 Hz - 100 kHz) in [67] after one stage with a compression factor of 8, by 1.4 (1 Hz - 10 kHz) after one stage with a compression factor of 11 in [47] and

#259068 Received 17 Feb 2016; revised 24 Mar 2016; accepted 29 Mar 2016; published 20 Apr 2016

by 2.2 (1 Hz - 10 kHz) after a double-stage compression with an overall compression factor of 27 in [47]. On contrary, the intensity noise in the presented bulk broadening experiments is independent of the broadening factor. This is especially advantageous with respect to applications in nonlinear optics where CEP stabilization is required. Judging from the authors' experience, high-power SPM based bulk broadening is superior over any fiber technique in terms of applicability and reliability, in particular over kagomé-type lattice HC-PCFs. Moreover, bulk broadening is attractive for industrial applications where cost factor and robustness play decisive roles, too.

The possibility of WLC generation was shown. However, several drawbacks like the dependence on the input pulse duration, the observed instabilities and the need for cooling, resp. limit the applicability of filamentation for high power sources. Simulations with a 0.5 mm plate show that purely SPM based broadening is applicable to any MW peak power level and any pulse duration up to the ps order. Moreover, crystals that serve as Kerr media in TD oscillators withstand average powers of more than 1 kW [27, 28] and hence the approach is also average power scalable. Since multiple stage broadening allows to access the few-cycle pulse regime, the method is expected to be employed in seed generation of the third generation of femtosecond technology [16].

The decoupling of spatial and temporal nonlinear effects by means of introducing a guiding structure was revealed to be essential for peak power scaling of the approach. While first ideas of realizing this were rather complex [68], the method proposed in [54] is simple and was already successfully applied for GW level pulses [42]. The simulations show that it can be transferred to SPM based spectral broadening and lower peak power levels which match the current generation of fiber and innoslab amplifiers as well as TD oscillators [21–28]. The efficiency in the case of 10 μJ, 250 fs pulses was increased from 4 % in the single plate geometry to 40 % in an assembly of ten 0.5 mm thick plates. Further improvements are expected by optimizing plate thicknesses and distances to maximize the homogenization effect in the gaps. The 40 % efficiency is about a factor of two below the efficiencies of fiber technologies. In the light of the rapidly increasing peak powers of disk, fiber and slab sources, this factor appears compensable. The FTL is inversely proportional to the number of plates if dispersion is negligible. Simulations show that the broadening factor in a single thin plate is constant for a fixed peak power, crystal length and damage threshold, i.e. independent of the input pulse duration. This makes intermediate compression after a few plates attractive for achieving very high compression factors.

6. Conclusion

In conclusion, spectral broadening in bulk material with average powers of 50 W was demonstrated. Broadening and compression factors of about 6 with a single plate were reached with a 60 % efficiency. To the best of the authors' knowledge, this marks a unique combination of unprecedented high compression factors and efficiencies together with an average power which is way beyond those of previously described bulk broadening experiments [36, 64, 68].

Furthermore, the evolution of temporal phase with respect to the broadening factor was analyzed by means of FROG measurements and the coupling between spatial losses and broadening was investigated with respect to peak power by means of full 3D simulations which reproduce the experimental results well. The trade-off between broadening factor and efficiency was pointed out as well as the limited peak power scalability of the single plate approach. The presented experiments show that multiple bulk broadening stages with intermediate compression allow to go from pulse durations of about 250 fs to the few-cycle regime. Simulations predict that the SPM based approach is also applicable for longer pulse durations which is important for Yb:YAG based amplifiers and SESAM mode-locked TD oscillators.

#259068 Received 17 Feb 2016; revised 24 Mar 2016; accepted 29 Mar 2016; published 20 Apr 2016

The multiple thin plate approach is also applicable to pure SPM based broadening of pulses with peak power levels beyond the power for critical self-focusing. It has been demonstrated that the quasi guiding structure, introduced by air gaps between the plates, leads to homogenizing of the spectrum over the beam area and thus to significantly reduced losses. Moreover, contrary to the single plate approach, simulations with the multiple plate geometry show that the losses do not scale with peak power anymore. Consequently, ionization-free bulk broadening has proved to be scalable not only in average power but also in peak power. Eventually, the noise properties of the approach have been investigated. The intensity noise remained on the low level of the TD oscillator and was independent of the broadening factor. This is in particular highly favorable in comparison to measurements performed after spectral broadening in kagomé-type HC-PCFs [47].

These findings combined with low costs, high robustness and alignment insensitivity, make the approach extremely attractive for pulse compression of high peak and average power light sources.

Acknowledgments

The authors gratefully acknowledge many fruitful discussions with Ferenc Krausz. The research was supported by the Munich-Centre for Advanced Photonics (MAP).

#259068 Received 17 Feb 2016; revised 24 Mar 2016; accepted 29 Mar 2016; published 20 Apr 2016